Baryon stopping and strange baryon and antibaryon production at ultrarelativistic energies

H. Weber, E. L. Bratkovskaya,* and H. Stöcker

Institut für Theoretische Physik, Universität Frankfurt, D-60054 Frankfurt am Mine, Germany
(Received 12 May 2002; revised manuscript received 26 August 2002; published 27 November 2002)

The amount of proton stopping in central Pb+Pb collisions from 20–160 A GeV as well as hyperon and antihyperon rapidity distributions are calculated within the UrQMD model in comparison to experimental data at 40, 80, and 160 A GeV taken recently from the NA49 collaboration. Furthermore, the amount of baryon stopping at 160A GeV for Pb+Pb collisions is studied as a function of centrality in comparison to the NA49 data. We find that the strange baryon yield is reasonably described for central collisions, however, the rapidity distributions are somewhat more narrow than the data. Moreover, the experimental antihyperon rapidity distributions at 40, 80, and 160 A GeV are underestimated by up to factors of 3—depending on the annihilation cross section employed—which might be addressed to missing multimeson fusion channels in the UrQMD model.

I. INTRODUCTION

Present lattice QCD calculations indicate that strongly interacting hadronic matter at temperatures of 150–170 MeV (or energy densities of 1–2 GeV/fm^3) should undergo a phase transition to a new state of matter generally denoted as quark-gluon plasma (QGP). It is also a common believe that this state of matter existed during the early phase of the universe until the temperature drop due to the rapid expansion lead to the freeze-out of hadrons which constitute a sizable fraction of the total mass of the universe. Whereas the ''big bang'' has only been a single event—for presently living observers—relativistic collisions of heavy nuclei, offer the unique possibility to study the dynamics of a huge number of ''tiny bangs'' under well controlled laboratory conditions. Hadronic spectra and relative hadron abundancies reflect the dynamics in the hot and dense zone formed in the early phase of the reaction.

Whereas meson rapidity distributions and transverse mass spectra essentially reflect the dynamics of newly produced $q\bar{q}$ pairs, the baryon rapidity, and transverse mass distributions give important information on baryon stopping [1] whereas antibaryon abundancies shed some light on quark chemical potentials μ_q at the space-time points of chemical decoupling, i.e., when chemical reactions no longer occur due to a large average separation between the hadrons. The latter statement, however, only holds if an approximate chemical equilibrium is reached in the collision zone of nucleus-nucleus reactions. In fact, chemical equilibrium models—based on extrapolations of existing data at the alternating-gradient synchroton (AGS) and SPS—suggest that the highest strange baryon abundancies should occur in central collisions of heavy nuclei between 20 and 40 A GeV [2]. Furthermore, the degree of baryon stopping is related (by energy-momentum conservation) to the number of newly produced hadrons dN/dy (per unit rapidity) which can be used to extrapolate the achieved energy density in these collisions by adopting the Bjoken formula [3]

$$\epsilon = \frac{M_T}{\tau_0 A} \frac{dN}{dy}\Big|_{y=y_{c.m.}}, \qquad (1)$$

where A is the transverse (geometrical) overlap region, M_T is the average transverse mass and τ_0 being the proper production time which is estimated to be in the order of 1 fm/c. According to Eq. (1) the energy densities reached in central Pb+Pb collisions at the SPS—using experimental infor-

mation on M_T and $dN(y_{c.m.})/dy$ should be in the order of 2.5–3.5 GeV/fm^3, i.e., well above the critical energy density for a transition to a QGP in equilibrium.

The data from the SPS on baryon stopping demonstrate that simple extrapolations from pp collisions at the same energy do not show enough baryon stopping (cf. e.g., Refs. [4,5]). Here transport models employing hadronic and string degrees-of-freedom such as RQMD [6], UrQMD [7,8], or HSD [9,10] do a better job since the formation and multiple rescattering of formed hadrons are included in these approaches. Furthermore, such transport calculations allow to study the change in dynamics from elementary baryon-baryon or meson-baryon collisions to proton-nucleus reactions or from peripheral to central nucleus-nucleus collisions in a unique way without changing any parameter. This is of central importance since the prejudice of thermal and chemical equilibrium does not hold in all of these reactions, and the transport studies allow to explore the amount of (thermal or chemical) equilibrium reached in such collisions [11,12].

Experimentally, the dynamics of heavy nucleus-nucleus collisions have been studied up to 11.6A GeV at the BNL AGS and an extensive program has been carried out at the ''top'' CERN SPS energy of 160A GeV, whereas the intermediate range from 11 to 160 A GeV has been practically unexplored from the experimental side. Only recently, experiments for Pb+Pb collisions at 40 and 80 A GeV have been performed at the CERN SPS [13,14] and further experimental measurements are expected at 20A GeV [15]. In this respect there is considerable hope that the experimental data can throw light on the basic question—if we might find signatures for an intermediate QGP state or if we just see strongly interacting hadronic matter.

In a previous study—within the UrQMD approach—we have addressed pion, kaon, and antikaon abundancies and spectra in central Pb+Pb collisions from 20–160 A GeV in comparison to the data from the NA49 Collaboration [16]. In general, we have found that the UrQMD model reasonably describes the data, however, systematically overpredicts the π^- yield by $\sim 20\%$, whereas the K^+ yield is underestimated by $\sim 15\%$. The K^- yields are in a good agreement with the data for all energies. This suggests that the production of antistrange quarks ($\bar{s}$) might be somewhat low in the transport model (as in the HSD approach [9]) whereas the production of the lightest $q\bar{q}$ pairs is overestimated systematically. However, in order to obtain a complete information on the abundancy of $s, \bar{s}$ quarks one has to study strange baryon production and antihyperon production, too, since strangeness conservation implies the same amount of s and $\bar{s}$ quarks to be produced in the collision. It is the aim of this work to provide an answer to this question within nonequilibrium transport theory.

II. PROTON STOPPING AND HYPERON PRODUCTION

The UrQMD transport approach is described in Refs. [7,8] and includes all baryonic resonances up to an invariant mass of 2 GeV as well as mesonic resonances up to 1.9 GeV as tabulated in the Particle Data Group (PDG) [17]. For hadronic continuum excitations we employ a string model with meson formation times in the order of $1–2$ fm/c depending on the momentum and energy of the created hadrons. The transport approach is matched to reproduce the nucleon-nucleon, meson-nucleon, and meson-meson cross section data in a wide kinematical regime [7,8]. At the high energies considered here, the particles are essentially produced in primary high energetic collisions by string excitation and decay, however, the secondary interactions among produced particles (e.g., pions, nucleons, and excited baryonic and mesonic resonances) also contribute to the particle dynamics—in production as well as in absorption.

Here we can come directly to the results for baryons and antibaryons and start at the highest bombarding energy of $160A$ GeV. The comparison of the UrQMD results on baryon stopping for the most central Pb+Pb collisions at $160A$ GeV to the NA49 data [18] has been reported previously in Refs. [7,19]. In Fig. 1 we compare the UrQMD (version 1.3) calculations for the net proton rapidity distribution $p-\bar{p}$ to the most resent data from the NA49 Collaboration [20] for six different centrality classes of Pb+Pb collisions—from the most central (bin 1) to the very peripheral collisions (bin 6). Note, that the spectators are excluded from the calculated dN/dy spectra in line with the experimental measurement. We find that the UrQMD model overestimates the stopping for the most central rapidity bin, i.e., the data show a slight dip at midrapidity and a two peak stucture, which indicates that full stopping is not achieved at $160A$ GeV even for this heavy system. On the other hand, it is quite remarkable that the hadron/string approach well reproduces the $p-\bar{p}$ rapidity distributions as a function of centrality.

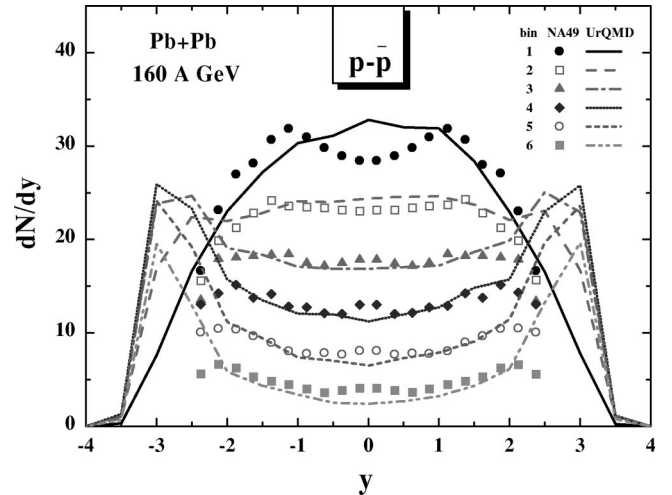We step on with the hyperon ($\Lambda+\Sigma^0$) rapidity distribu-

FIG. 1. The rapidity distribution of net protons $p-\bar{p}$ in Pb+Pb collisions at $160A$ GeV calculated within the UrQMD model (lines) in comparison to the experimental data from the NA49 Collaboration [20] for six different centrality classes—from the most central (bin 1) to the very peripheral collisions (bin 6).

tions at 40, 80, and 160 A GeV in comparison to the data from NA49 [14]—Fig. 2. The UrQMD calculations show an increasing hyperon yield with bombarding energy essentially due to a broadening of the rapidity distribution, while the midrapidity distributions at 40 and 80 A GeV are practically the same. The data from the NA49 Collaboration show a decreasing hyperon yield at midrapidity with higher bombarding energy while suggesting a slightly larger width in dN/dy. Note, however, that the data at $160A$ GeV correspond to 10% centrality whereas the lower energies are for 7% centrality, respectively. We mention that for 7% centrality our calculations at $160A$ GeV roughly give the same $\Lambda +\Sigma^0$ yield at midrapidity than for the lower energies of 40 and 80 A GeV. It is not clear at present from the data, if the total integrated yields are compatible with our calculations. However, as demonstrated in Ref. [16], the UrQMD model describes rather well the antikaon rapidity distributions from 40–160 A GeV whereas the kaon rapidity distributions are underestimated by about 15%. Consequently, by strangeness
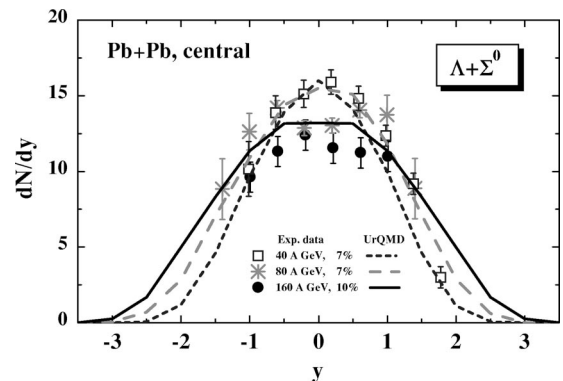

FIG. 2. The UrQMD calculations of the hyperon ($\Lambda+\Sigma^0$) rapidity distributions for Pb+Pb collisions at 40 (7% central), 80 (7% central), and 160 (10% central) A GeV in comparison to the data from the NA49 Collaboration [14].
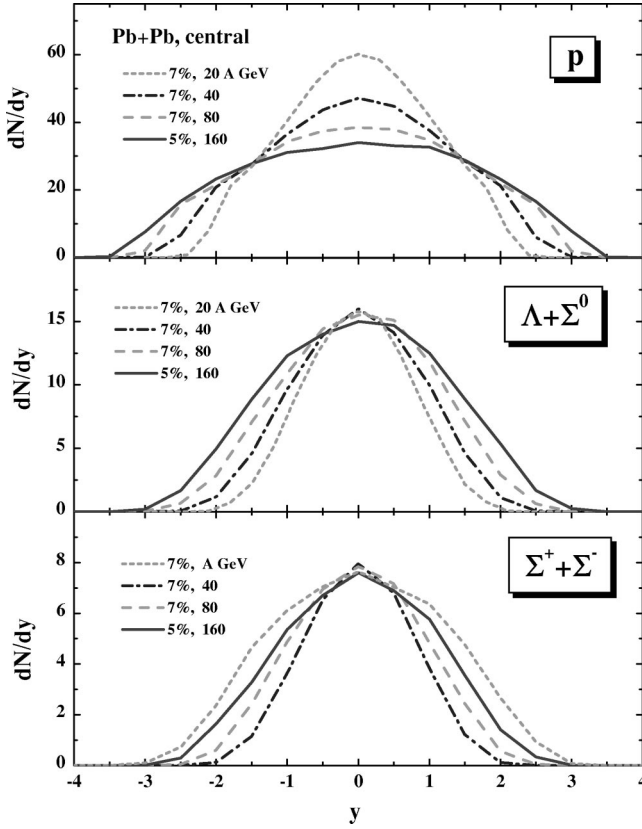
FIG. 3. The rapidity distributions of net protons $p - \bar{p}$, hyperons ($\Lambda + \Sigma^0$ and $\Sigma^+ + \Sigma^-$) calculated within the UrQMD model for 7% central Pb+Pb collisions at 20 (short-dashed lines), 40 (dot-dashed lines), 80 (dashed lines), and for 5% central collisions at 160A GeV (solid lines).

conservation, which is strictly fulfilled in the UrQMD approach, the hyperon yield should also be underestimated slightly.

We, furthermore, provide an overview on rapidity distributions of protons, neutral ($\Lambda + \Sigma^0$), and charged hyperons ($\Sigma^+ + \Sigma^-$) at 40, 80, and 160 A GeV from 7% or 5% central Pb+Pb collisions within the UrQMD model as well as predictions for 20A GeV (Fig. 3), where experimental measurements will be taken in near future [15]. Whereas the net proton density at midrapidity decreases strongly with higher bombarding energy—which should be attributed to a lower amount of baryon stopping—the width in rapidity increases accordingly since the net $p - \bar{p}$ number is a constant, if the produced meson system on average is charge neutral. The situation with strange baryons is different since a newly produced s quark is contained in their wave function. In the UrQMD transport model, this leads to a much narrower rapidity distribution for strange baryons than for protons from 20–160 A GeV as seen from Fig. 3. Consequently, the Λ/p ratio varies sensitively with rapidity.

III. ANTIPROTON AND ANTIHYPERON PRODUCTION

We continue with antibaryon production in central Pb+Pb collisions at SPS energies. Since the final $\bar{p}$ or $\bar{\Lambda}$ rapidity
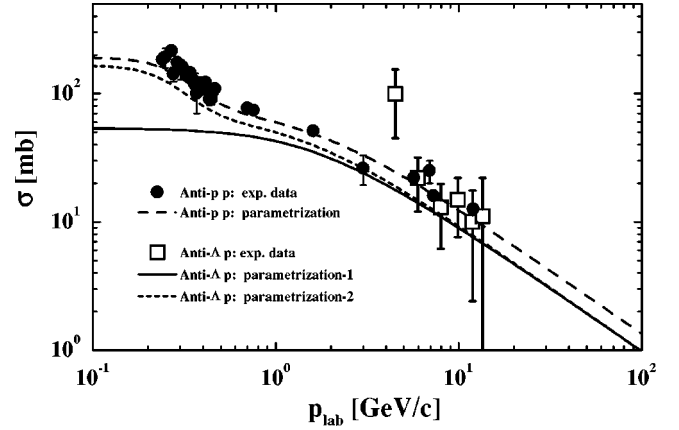

FIG. 4. The annihilation cross section of $\bar{p}$ and $\bar{\Lambda}$ with nucleons as a function of incident ($\bar{p}$ or $\bar{\Lambda}$) momentum in the laboratory frame. The solid circles are the $\bar{p}$ data from Ref. [17], the open squares correspond to the $\bar{\Lambda}p$ data from Ref. [21]. The dashed line is the parametrization of the $\bar{p}$ annihilation cross section used in UrQMD, the short-dashed and solid lines correspond to the two different parametrizations of the $\bar{\Lambda}p$ data (see text).

distributions are sensitive to their annihilation cross section with nucleons, we first discuss the actual implementation of annihilation within UrQMD. In this respect we show in Fig. 4 the annihilation cross section of $\bar{p}$ and $\bar{\Lambda}$ with nucleons as a function of the incident ($\bar{p}$ or $\bar{\Lambda}$) momentum in the laboratory frame. The solid circles are the $\bar{p}$ data from Ref. [17] while the open squares correspond to the $\bar{\Lambda}p$ data from Ref. [21]. The dashed line stands for the parametrization of the $\bar{p}$ annihilation cross section used in UrQMD while the short-dashed and solid lines correspond to two different parametrizations of the $\bar{\Lambda}p$ annihilation cross section, which are both compatible to the experimental data (open squares), however, involve quite different extrapolations to the low momentum regime. The parametrization-1 (short-dashed line) assumes

$$\sigma_{\bar{\Lambda}N}^{ann}(\sqrt{s}) \approx 0.8 \sigma_{\bar{p}N}^{ann}(\sqrt{s}), \qquad (2)$$

thus relating the different cross sections at the same invariant energy $\sqrt{s}$, which leads to a constant annihilation cross section for antilambdas at low momentum of ≈ 55 mb (default in UrQMD). The parametrization 2 (solid line) instead assumes

$$\sigma_{\bar{\Lambda}N}^{ann}(p_{lab}) \approx 0.8 \sigma_{\bar{p}N}^{ann}(p_{lab}), \qquad (3)$$

thus relating the different cross sections at the same laboratory momentum p_{lab}. We note again that the data on $\bar{\Lambda}$ annihilation at high momenta are compatible with both parametrizations.

The UrQMD calculations of the antiproton ($\bar{p}$) rapidity distribution for 5% central Pb+Pb collisions at 160A GeV are shown in Fig. 5 in comparison to the data from the NA49 Collaboration [22], which also include some contribution from the feeddown of $\bar{\Lambda}$ and $\bar{\Sigma}^0$. The experimental distribution is underestimated severely in UrQMD suggesting either
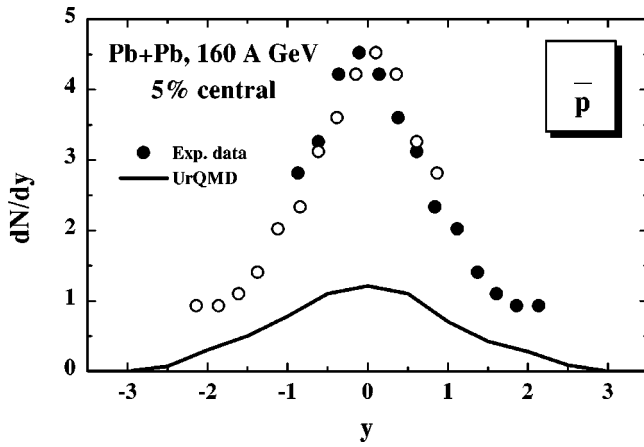
FIG. 5. The UrQMD calculations of the antiproton ($\bar{p}$) rapidity distribution for 5% central Pb+Pb collisions at 160A GeV in comparison to the data from the NA49 Collaboration [22].

a much lower annihilation cross section for antiprotons or the dominance of multimeson fusion channels as suggested in Refs. [24–26].

Within the strangeness balance discussed in the context with Figs. 2 and 3, the antistrangeness content of antihyper-
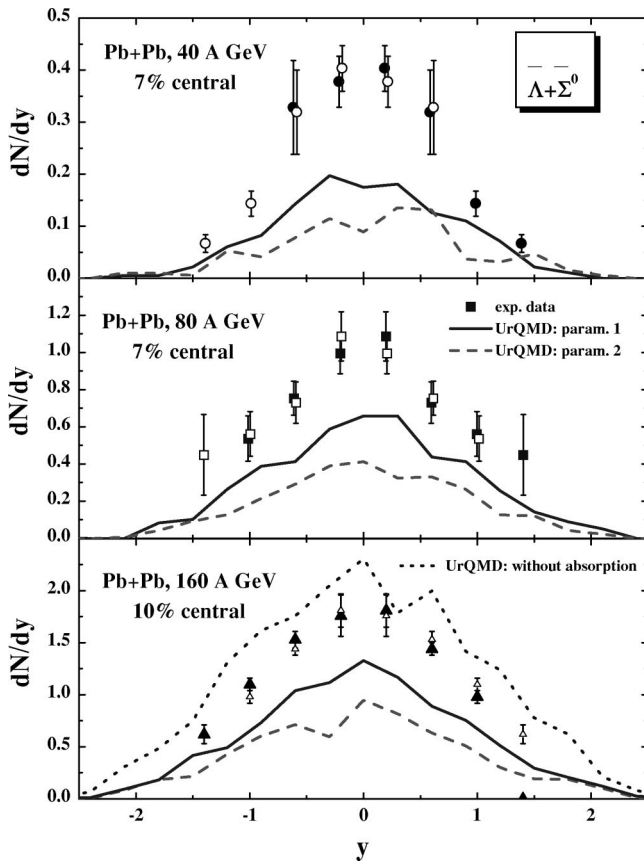

FIG. 6. The UrQMD calculations of the antihyperon ($\bar{\Lambda}+\bar{\Sigma}^0$) rapidity distributions for 7% central Pb+Pb collisions at 40 and 80 A GeV and for 10% central Pb+Pb at 160A GeV in comparison to the data from the NA49 Collaboration [14,23]. The short-dashed line for 160A GeV corresponds to a calculation without antihyperon annihilation.
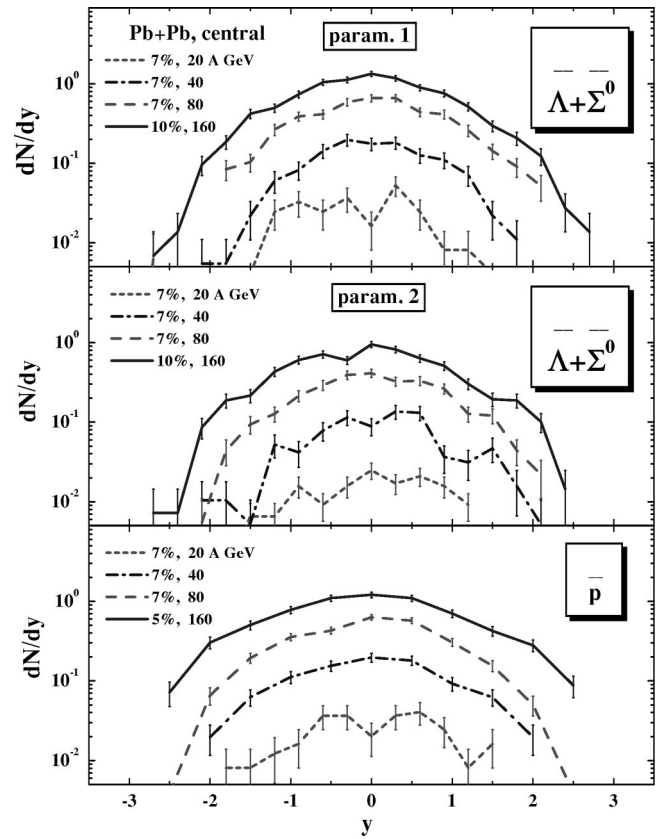

FIG. 7. The rapidity distributions of antihyperons ($\bar{\Lambda}+\bar{\Sigma}^0$) and antiprotons ($\bar{p}$) calculated within the UrQMD model for 7% central Pb+Pb collisions at 20 (short dashed lines), 40 (dot-dashed lines), 80 (dashed lines), and for 10% central ($\bar{\Lambda}+\bar{\Sigma}^0$) or 5% central collisions (for $\bar{p}$) at 160A GeV (solid lines). The upper plot corresponds to the parametrization-1 for $\bar{\Lambda}p$ annihilation cross section whereas the middle plot shows the UrQMD results with the "parametrization-2" (see text).

ons ($\bar{\Lambda}+\bar{\Sigma}$) has been neglected. This conjecture remains to be proven. In fact, as shown in Fig. 6, the experimental data [14,23] for central Pb+Pb collisions at 80A GeV give $dN/dy\approx 1$, which is within the experimental error bars for $\Lambda+\Sigma^0$ in Fig. 2. This even more holds true at the lower bombarding energy of 40A GeV. The UrQMD calculations for the same centrality bin underestimate the NA49 data [14] by about a factor of 2 (for parametrization 1) or 3 (for parametrization 3) at 40 and 80 A GeV whereas the data at 160A GeV are underestimated only by about factors of 1.5–2. The short-dashed line (in the lower part for 160A GeV) shows the result of a calculation without antihyperon annihilation which only slightly overestimates the data. When integrating over rapidity we find that in case of parametrization 1 about half of the antihyperons are annihilated whereas for the parametrizarion 2~2/3 of the antihyperons disappear.

It has been shown previously in Ref. [27] that the standard UrQMD model (with parametrization-1) underestimates the (multi)strange baryon multiplicity for central Pb+Pb at 160A GeV. As argued in Ref. [27], the inclusion of nonhadronic medium effects, such as color-ropes [28] (simulated in UrQMD by increasing the string tension), enhances the mul-

tiplicity of (anti)strange baryons. The missing antihyperon yield can be attributed also to multimeson fusion channels involving $K, \bar{K}, K^+, \bar{K}^*$ mesons [25,26] that are not accounted for in the calculations reported here. Furthermore, the high abundance of Ω and $\bar{\Omega}$ seen experimentally might also signal the appearance of disoriented chiral condensates (DCC's) as put forward by Kapusta and Wong [29]. In short, this issue is presently still open.

In order to provide an overview on antiproton and antihyperon production (in analogy to Fig. 3) we show in Fig. 7 the rapidity distributions of antihyperons $(\bar{\Lambda} + \bar{\Sigma}^0)$ calculated within the UrQMD model for 7% central Pb+Pb collisions at 20 (short dashed lines), 40 (dot-dashed lines), 80 (dashed lines), and for 10% central $(\bar{\Lambda} + \bar{\Sigma}^0)$ and 5% central $(\bar{p})$ collisions at $160A$ GeV (solid lines). The upper plot corresponds to the "parametrization 1" for $\bar{\Lambda}p$ annihilation cross section whereas the middle plot shows the UrQMD results with the "parametrization 2." The abundancy of strange antibaryons $(\bar{\Lambda} + \bar{\Sigma}^0)$ increases rapidly with bombarding energy. Note, since the antihyperon yield is very low especially at $20A$ GeV, we present the antihyperon rapidity distribution in a logarithmic scale and indicate the statistical errorbars in order to demonstrate the accuracy/statistics achieved in the UrQMD calculations. As discussed above the antihyperon absorption is more pronounced for parametrization-2 especially at lower bombarding energy. We note in passing, that the (rapidity integrated) $\bar{\Lambda}/\bar{p}$ ratio from the UrQMD calcu-

lation is ~ 0.9 and 0.6 for all bombarding energies from 20–160 A GeV within the parametersets 1 and 2, respectively.

IV. CONCLUSIONS

In summary, we have calculated the amount of baryon stopping in central Pb+Pb collisions from 20–160 A GeV as well as hyperon rapidity distributions in comparison to experimental data at 40, 80, and 160 A GeV taken recently by the NA49 collaboration [14]. We have demonstrated, furthermore, that the UrQMD model reasonably reproduces the amount of baryon stopping at $160A$ GeV for Pb+Pb collisions as a function of centrality. The comparison of our calculations for hyperons with the experimental data, however, indicates that the strange baryon yield at midrapidity is slightly overestimated whereas the calculated rapidity distributions are somewhat more narrow than the data. This discrepancy might indicate a different mechanism for strange hyperon production than the string mechanism in the transport model. On the other hand, the experimental antihyperon rapidity distributions at 40, 80, and 160 A GeV as well as the antiproton rapidity distribution at $160A$ GeV are underestimated by up to factors of 3 which we address to missing multimeson fusion channels [24–26] in the UrQMD model. Note, however, that instead of multimeson fusion channels, also disoriented chiral condensates might explain the enhanced production of multistrange baryons as suggested in Ref. [29].

[1] W. Scheid, R. Ligensa, and W. Greiner, Phys. Rev. Lett. **21**, 1479 (1968).

[2] P. Braun-Munzinger, J. Cleymans, H. Oeschler, and K. Redlich, Nucl. Phys. **A697**, 902 (2002).

[3] J. D. Bjorken, Phys. Rev. D **27**, 140 (1983).

[4] *Quark Matter 1999* [Nucl. Phys. **A661**, 1 (1999)].

[5] *Quark Matter 2001* [Nucl. Phys. **A698**, 1 (2001)].

[6] F. Wang, H. Liu, H. Sorge, N. Xu, and J. Yang, Phys. Rev. C **61**, 064904 (2000).

[7] S. A. Bass *et al.*, Prog. Part. Nucl. Phys. **42**, 279 (1998).

[8] M. Bleicher *et al.*, J. Phys. G **25**, 1859 (1999).

[9] J. Geiss, W. Cassing, and C. Greiner, Nucl. Phys. **A644**, 107 (1998).

[10] W. Cassing and E. L. Bratkovskaya, Phys. Rep. **308**, 65 (1999).

[11] E. L. Bratkovskaya *et al.*, Nucl. Phys. **A675**, 661 (2000).

[12] M. Belkacem *et al.*, Phys. Rev. C **58**, 1727 (1998); L. V. Bravina *et al.*, Phys. Lett. B **434**, 379 (1998); L. V. Bravina *et al.*, J. Phys. G **25**, 351 (1999); L. V. Bravina *et al.*, Phys. Rev. C **60**, 024904 (1999).

[13] S. V. Afanasiev *et al.*, nucl-ex/0205002.

[14] A. Mischke *et al.*, J. Phys. G. **28**, 1761 (2002).

[15] The NA49 Collaboration, Addendum-10 to Proposal CERN/ SPSC/P264, "Progress Report and Beam Request for 2002."

[16] H. Weber, E. L. Bratkovskaya, and H. Stöcker, nucl-th/0205030, Phys. Lett. B (in press).

[17] Particle Data Group, D. E. Groom *et al.*, Eur. Phys. J. C **15**, 1 (2000).

[18] H. Appelshäuser *et al.*, Phys. Rev. Lett. **82**, 2471 (1999).

[19] S. A. Bass, M. Gyulassy, H. Stöcker, and W. Greiner, J. Phys. G **25**, R1 (1999).

[20] C. E. Cooper *et al.*, Nucl. Phys. **A661**, 362c (1999).

[21] F. Eisele *et al.*, Phys. Lett. **60B**, 297 (1976); **60B**, 1067 (1976).

[22] J. Bächler *et al.*, Nucl. Phys. **A661**, 45c (1999).

[23] A. Mischke *et al.*, nucl-ex/0209002.

[24] R. Rapp and E. V. Shuryak, Phys. Rev. Lett. **86**, 2980 (2001).

[25] C. Greiner and S. Leupold, J. Phys. G **27**, L95 (2001).

[26] W. Cassing, Nucl. Phys. **A700**, 618 (2002).

[27] S. Soff *et al.*, Phys. Lett. B **471**, 89 (1999).

[28] T. S. Biro, H. B. Nielsen, and J. Knoll, Nucl. Phys. **B245**, 449 (1984); H. Sorge, M. Berenguer, H. Stöcker, and W. Greiner, Phys. Lett. B **289**, 6 (1992); S. E. Vance and M. Gyulassy, Phys. Rev. Lett. **83**, 1735 (1999).

[29] J. I. Kapusta and S. M. H. Wong, Phys. Rev. Lett. **86**, 4251 (2001).